Phys. Status Solidi B **247**, No. 5, 1095–1098 (2010) / **DOI** 10.1002/pssb.200945486

physica status solidi b
www.pss-b.com
basic solid state physics

Energy-resolved STM maps of finite carbon nanotubes and the role of surface–tube interactions

Mario De Menech[1,2], Ulf Saalmann[1], and Martin E. Garcia[*,2]

[1] Max-Planck-Institut für Physik komplexer Systeme, Nöthnitzer Str. 38, 01187 Dresden, Germany
[2] Theoretische Physik, Fachbereich 18, Universität Kassel and Center for Interdisciplinary Nanostructure Science and Technology (CINSaT), Heinrich-Plett-Str. 40, 34132 Kassel, Germany

Received 21 October 2009, revised 12 January 2010, accepted 29 January 2010
Published online 24 March 2010

PACS 73.22.–f, 73.40.Gk, 73.63.–b

[*] Corresponding author: e-mail garcia@physik.uni-kassel.de, Phone: +49-561-804-4480, Fax: +49-561-804-4006

The influence of the supporting surface on the standing wave electronic modes of finite metallic carbon nanotubes (CNTs) is discussed. The charge distribution of the states is visualized by simulating the energy resolved scanning tunneling spectroscopy (STS) maps. The Fourier transform of the spatial patterns exhibited by the STS maps allows to reconstruct the dispersion relation, whose definiteness is smeared out for increasing surface–tube interaction strengths. The scattering of the modes in the tube due to the interaction with the surface causes distortions of the simulated maps. For example, the reflection symmetry with respect to the mirror plane perpendicular to the tube axis appears to be broken for modes in the case of narrow tubes, when the interaction with the surface is strong enough.

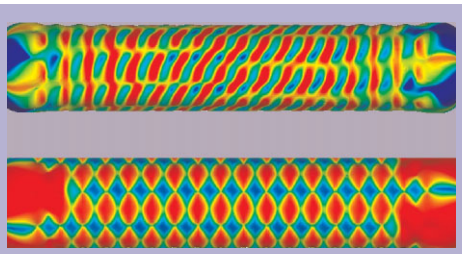

Breaking of the reflection symmetry: STS map for a (4,4) carbon nanotube of length $50a_0$ near the Fermi level placed at 2.5 Å (upper tube) and 3.0 Å (lower tube) away from an Au(111) surface. Red, green, and blue colored regions refer to large, intermediate and low values of the current, respectively.

1 Introduction An effective use of carbon nanotubes (CNTs) for nanoelectronics applications cannot be successful without a throughout understanding of the coupling to metallic contacts. Moreover, assuming that such nanodevices do not consist of free standing nanotubes but of supported ones, the influence of the substrate must be determined, *e.g.*, in Ref. [1]. In this paper we illustrate how the scanning tunneling spectroscopy (STS) mapping can be used to investigate the nature of the CNT–surface interaction. In particular we consider the influence of the nanotube–surface interaction on the standing electronic wave modes of finite CNTs.

Venema et al. [2] first reported investigations of quantum size effects in armchair 30 nm long CNTs; Odom et al. [3] have investigated with scanning tunneling microscopy (STM) technique even shorter tubes, down to 3 nm. Lemay et al. [4] have obtained two-dimensional (2D) STS images of CNTs on Au(111) surfaces, which were strongly affected by the scattering at the defects (both at the ends or along the tube), with the mixing of the bonding and antibonding modes, as described by Kane and Mele [5]. From the Fourier analysis of the images they could get the linear dispersion relation near the Fermi energy, based on the longer wavelength modes. The same result was obtained by Ouyang et al. [6] looking at the decay of the scattered wave from a defect on a tube supported by an Au surface. They define a phenomenological coherence length $l_\varphi \approx 1$ nm which gives the decay of the interference pattern between the incoming and reflected wave. The measured l_φ is much smaller than the coherence length measured in transport experiments. Yang et al. [7] proposed that l_φ just gives a measure of the localization of the defect state. The approach used in Ref. [6] should be quite common in the description of the reflection of 2D surface states

at linear defects on metal surfaces. More recently, Lee et al. [8] have analyzed the reflection of waves at the end of a CNT, providing the evidence of a Luttinger liquid behavior.

In this paper we simulate the STS energy-resolved imaging of finite armchair CNTs on Au(111) surfaces based on both the tube's topography and the local density of states (LDOS). We show that even for very short tubes (down to 20 unit cells) the energy–momentum dispersion relation of the propagating modes can be clearly identified from the STS maps. We discuss how the strength of the coupling to the Au(111) surface affects the band structure of the CNTs. Breaking of the reflection symmetry is observed for perfect narrow tubes for strong nanotube–surface interaction.

The paper is organized as follows. The theoretical framework, presented in a previous publication [9], is only very briefly reviewed in Section 2. The experienced reader may skip this part and move directly to the results, shown in Section 3.

2 Theory To determine the STM maps we use a theoretical approach which we developed and applied to supported Ag_n clusters [10, 11] and C_{60} molecules [10]. We have also studied, using this method and experimental data, tip-induced distortions of STM images in CNTs on highly-ordered pyrolytic graphite (HOPG) surfaces [12].

In short, the electronic properties of the surface, the STM probe and the CNT sample are described within the single-particle picture, based on a tight-binding (TB) model with self-consistent charge, whose parameterization is computed from DFT-LDA [13]. The equilibrium properties of the CNT are calculated using Green's function methods. The interaction of the tube with the supporting substrate is included through self-energy terms in the CNT retarded Green's function G, from which one can construct the density of states (DOS) the LDOS

$$\rho(\boldsymbol{r}, E) = -\frac{2}{\pi}\sum_{\mu\nu} \mathrm{Im}[G_{\mu\nu}(E)]\varphi_\mu(\boldsymbol{r})\varphi_\nu(\boldsymbol{r}), \tag{1}$$

where the functions $\varphi_\mu(\boldsymbol{r})$ represent the atomic orbitals of the TB model. Within Tersoff–Hamann theory [14, 15], the STM topographic and spectral images are modeled assuming that the current at bias V is proportional to the spatially resolved DOS:

$$I(\boldsymbol{r}, V) \propto \int_{E_\mathrm{F}}^{E_\mathrm{F}+|e|V} \mathrm{d}E\ \rho(\boldsymbol{r}, E). \tag{2}$$

Equation (2) allows to calculate the tip trajectory, based on the assumption that the convolution effects due to the tip shape and states can be neglected. The local differential conductance $\mathrm{d}I(\boldsymbol{r}, V)/\mathrm{d}V \propto \rho(\boldsymbol{r}, E)\infty$ can be projected on the iso-current surface to simulate the experimental procedure followed to measure STS maps. This method has been successfully applied to metallic clusters on graphite surfaces [10].

3 Results Armchair CNTs are uniquely identified by their diameter, and can be constructed by wrapping a graphene sheet along the direction $n(\boldsymbol{e}_1 + \boldsymbol{e}_2)$, where $\boldsymbol{e}_1$ and $\boldsymbol{e}_2$ are the base vectors of the graphene sheet [16]. The unit cell of the tube is a ring formed by $4n$ atoms, $a_0 = 1.42\sqrt{3}\,\text{Å} = 2.4\,\text{Å}$ long. The band structure and the eigenfunctions of an armchair tube can be derived with a simple Hückel model, considering a unit cell made by four consecutive atoms along the armchair, with a single parameter γ corresponding to the π orbital hopping element between two neighboring carbon atoms. The Fermi level is placed at the crossing of two linear bands. The bonding and antibonding character of the band states is related to the lack or presence of nodes in the transverse direction, respectively. For an infinite tube, the eigenfunctions take the form $\psi_i = c_i \exp(ikz)$, $i = 1, 2, 3, 4$; and in a finite tube only a discrete number of wavevectors are allowed: the resulting DOS is a combination the standing waves built from bonding and antibonding modes [17].

Figure 1 shows the simulated STS images for an (8,8) nanotube consisting of 30 unit repeat lengths in the energy range within the metallic plateau. This is the region of the DOS between the first van-Hove singularities located on each side of the Fermi energy. Figure 1 clearly shows that the STS maps are characterized by spatial periodic patterns associated whereby the standing waves in the finite tubes are clearly visible. Their wavelengths and apparent forms change with the energy.

3.1 Reconstruction of the dispersion relation The Fourier analysis of both the simulated vertical displacement of the tip and the LDOS projected on the topographic surface as a function of energy allows to relate the modes in the finite tubes to the band structure of the infinite CNTs. The LDOS corresponds the square of the wavefunction representing the state picked up by the tip, *cf.* Eq. (1). Due to this fact, an electronic wave function corresponding to a standing wave with wavenumber k will generate spatial oscillations in the LDOS having twice that frequency.

In Fig. 2 we summarize the analysis of energy-resolved maps for an (8,8) tube with $N = 20$ unit cells within an energy interval of about 1 eV from the Fermi level of the Au substrate. Figure 2a shows the absolute value of the Fourier transform of the oscillation of the probe height as it is moved in the longitudinal direction. Note, that the mode $k_0 = 2\pi/a_0$ corresponding to the periodicity of the unit cell is quite marked, regardless of the energy value. The longer wavelength modes associated with the linear dispersion of the bonding and antibonding modes are quite evident. Similar to Fig. 2a, Fig. 2b shows the Fourier transform of the projected LDOS on the simulated constant current surface, averaging out the absolute spectra in the transverse direction. The correspondence with the dispersion relation of the infinite tube appears even more clearly. In particular, it is possible to identify unambiguously a few allowed k values corresponding to the bonding (descending) band, which are

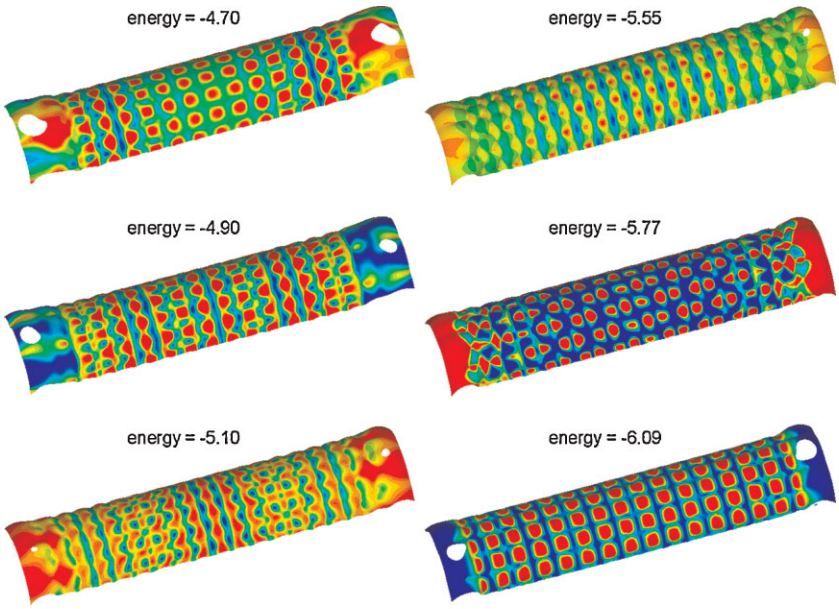

Figure 1 (online colour at: www.pss-b.com) STS maps of a (8,8) CNT with a length of $30a_0$ on an Au(111) surface at different energies (in eV) within the energy interval between the van-Hove singularities above and below the Fermi level (metallic plateau). a_0 is the length of a unit cell. Red, green, and blue colored regions refer to large, intermediate and low values of the current, respectively.

marked as $\pi_1, \pi_2, \pi_3, \pi_4$ in Fig. 2b. These modes are indicated also in the DOS of the central part of the tube in Fig. 2c. The additional Fourier peaks at $\pi_{1'}$ and $\pi_{2'}$ mirror the π_1 and π_2 modes: they are present due to the composition of the z-displacement mode k_0 mentioned above and the LDOS oscillations, generating the beating frequencies $|k_{\pi_1} - k_0|$ and $|k_{\pi_2} - k_0|$ which show up in the peaks $\pi_{1'}$ and $\pi_{2'}$.

3.2 Tube–surface interaction We studied how the interaction with the surface influences the reconstruction of the energy–momentum dispersion relation from the Fourier analysis of the local DOS. Figure 3 shows the Fourier analysis of the STS maps for (4,4) $N = 30$ tube placed at a distance of 2.5 Å (panel a) and 3.0 Å (panel b) from the gold substrate. As the strength of the interaction is decreased (increasing distance) the dispersion relation appears more definite, the peaks of the main mode in the Fourier transform gets sharper. The effect of the interaction on the broadening of the modes is less marked for larger tubes. Figure 4 displays the computed dispersion relation for a (8,8) tube with $N = 30$ placed at 2.5 and 3.0 Å from the surface: the allowed states can be recognized in both cases. Compared to the narrow (4,4) tube in Fig. 3, there is little difference in the broadening of the dispersion relation for the two distances.

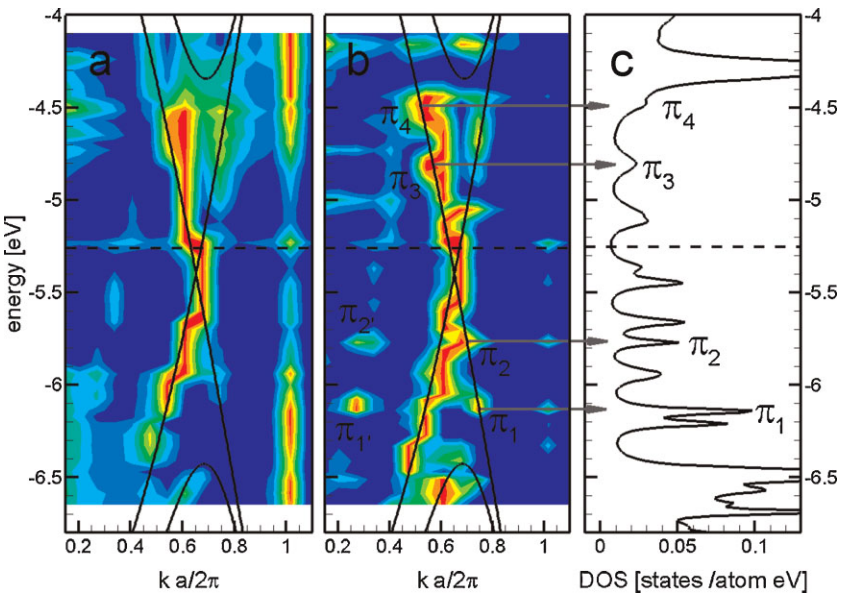

Figure 2 (online colour at: www.pss-b.com) Fourier analysis of the STM/STS maps of a (8,8) CNT of length $L = 20\ a_0 = 49.2$ Å on a Au(111) surface. (a) Topography, (b) energy-resolved map, and (c) DOS of the central part of the tube. The linear solid lines in (a) and (b) show the linear dispersion in the metallic plateau. The dashed line marks the Fermi level of the Au substrate (−5.26 eV). As in the case of the STS maps, the colors represent decrease in Fourier intensity from red to blue.

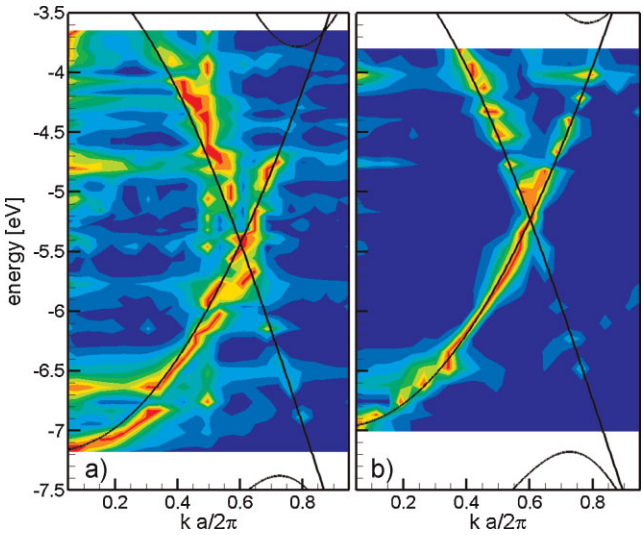

Figure 3 (online colour at: www.pss-b.com) Dispersion for (4,4) tubes with length $30\,a_0$ on an Au(111) surface, placed at 2.5 Å (panel a) and 3.0 Å (panel b). Solid lines show the band structure for an infinite tube. The color scale is the same as in the previous figures.

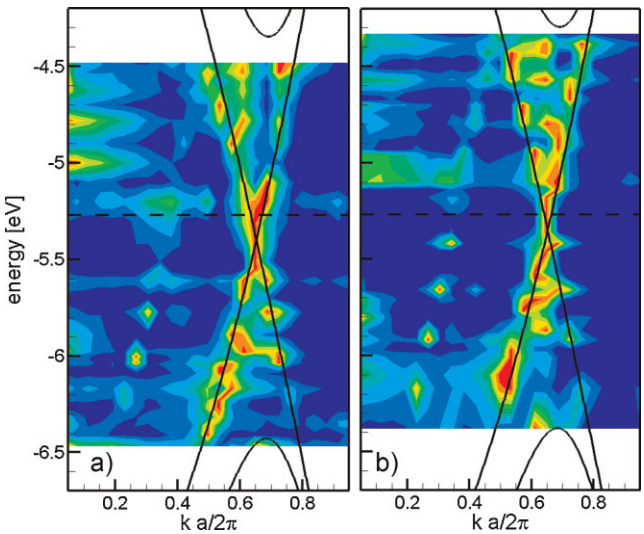

Figure 4 (online colour at: www.pss-b.com) Dispersion for (8,8) tubes with length $30a_0$ on an Au(111) surface, placed at 2.5 Å (panel a) and 3.0 Å (panel b). Solid lines show the band structure for an infinite tube. The color scale is the same as in the previous figures.

A sufficiently strong tube–surface interaction may even break the reflection symmetry for a perfect finite CNT.

4 Summary We presented calculations of STS maps of finite CNTs. In particular we concentrated on finite-size effects and on the influence of surface–tubes interactions on the images.

The observed standing-wave modes are symmetric, *i.e.*, possess the same symmetry properties as the underlying tubefor sufficiently large, weakly interacting tubes. Note that already (8,8) tubes with 30 repeat unit lengths fulfill this condition. In narrow, strongly coupled tubes symmetries, *cf. e.g.*, the reflection symmetry with respect to the mirror plane perpendicular to the tube axis in the abstract figure, may be broken.

The dispersion relations, derived from these modes, showalthough the CNT considered here contain only very few repeat unitssurprisingly good agreement with the band structure of the corresponding infinite tube. The deviations are in particular weak for ''broad'' nanotubes like the (8,8) CNT studied.

Acknowledgements We acknowledge financial support by the Deutsche Forschungsgemeinschaft (DFG) through the priority program SPP 1153 ''Clusters in contact with surfaces: Electronic structure and magnetism''.

References

[1] W. Orellana, Appl. Phys. Lett. **92**, 093109 (2008).
[2] L. C. Venema, J. W. C. Wildoer, J. W. Janssen, S. Tans, H. L. J. T. Tuinstra, L. P. Kouwenhoven, and C. Dekker, Science **283**, 52 (1999).
[3] T. W. Odom, J. L. Huang, P. Kim, and C. M. Lieber, J. Phys. Chem. B **104**, 2794 (2000).
[4] S. G. Lemay, J. W. Janssen, M. van den Hout, M. Mooij, M. J. Bronikowski, P. A. Willis, R. E. Smalley, L. P. Kouwenhoven, and C. Dekker, Nature **412**, 617 (2001).
[5] C. L. Kane and E. J. Mele, Phys. Rev. B **59**, R12759 (1999).
[6] T. W. Ouyang, J. L. Huang, and C. M. Lieber, Phys. Rev. Lett. **88**, 066804 (2002).
[7] H. T. Yang, J. W. Chen, L. F. Yang, and J. Dong, Phys. Rev. B **71**, 085402 (2005).
[8] J. Lee, S. Eggert, H. Kim, S. J. Kahng, H. Shinohara, and Y. Kuk, Phys. Rev. Lett. **93**, 166403 (2004).
[9] M. De Menech, U. Saalmann, and M. E. Garcia, Phys. Rev. B **73**, 155407 (2006).
[10] M. De Menech, U. Saalmann, and M. E. Garcia, Appl. Phys. A **82**, 113 (2006).
[11] M. De Menech, U. Saalmann, and M. E. Garcia, New J. Phys. **9**, 340 (2007).
[12] H. Hövel, M. De Menech, M. Bödecker, C. Rettig, U. Saalmann, and M. E. Garcia, Eur. Phys. J. D **45**, 459 (2007).
[13] M. Elstner, D. Porezag, G. Jungnickel, J. Elstner, M. Haugk, T. Frauenheim, S. Suhai, and G. Seifert, Phys. Rev. B **58**, 7260 (1998).
[14] J. Tersoff and D. R. Hamann, Phys. Rev. Lett. **50**, 1998 (1983).
[15] J. Tersoff and D. R. Hamann, Phys. Rev. B **31**, 805 (1985).
[16] R. Saito, M. S. Dresselhaus, and G. Dresselhaus (eds.), Physical Properties of Carbon Nanotubes (Imperial College Press, London, 1998).
[17] A. Rubio, D. Sanchez-Portal, E. Attach, E. Ordejon, and J. M. Soler, Phys. Rev. Lett. **82**, 3520 (1999).

